First publ. in: Molecular Microbiology 54 (2004), 3, pp. 647-664

Structure and assembly of the pseudopilin PulG

Rolf Köhler,[1†] Karsten Schäfer,[2†] Shirley Müller,[3†] Guillaume Vignon,[1] Kay Diederichs,[2] Ansgar Philippsen,[3] Philippe Ringler,[3] Anthony P. Pugsley,[1*] Andreas Engel[3] and Wolfram Welte[2]

[1]*Molecular Genetics Unit, Institut Pasteur, 25, rue du Dr Roux, 75724 Paris Cedex 15, France.*

[2]*Department of Biology, University of Konstanz, M656, D-78457 Konstanz, Germany.*

[3]*M. E. Müller Institute for Structural Biology, Biozentrum, University of Basel, CH-4056, Basel, Switzerland.*

Summary

The pseudopilin PulG is one of several essential components of the type II pullulanase secretion machinery (the Pul secreton) of the Gram-negative bacterium *Klebsiella oxytoca*. The sequence of the N-terminal 25 amino acids of the PulG precursor is hydrophobic and very similar to the corresponding region of type IV pilins. The structure of a truncated PulG (lacking the homologous region), as determined by X-ray crystallography, was found to include part of the long N-terminal α-helix and the four internal anti-parallel β-strands that characterize type IV pilins, but PulG lacks the highly variable loop region with a disulphide bond that is found in the latter. When overproduced, PulG forms flexible pili whose structural features, as visualized by electron microscopy, are similar to those of bacterial type IV pili. The average helical repeat comprises 17 PulG subunits and four helical turns. Electron microscopy and molecular modelling show that PulG probably assembles into left-handed helical pili with the long N-terminal α-helix tightly packed in the centre of the pilus. As in the type IV pilins, the hydrophobic N-terminal part of the PulG α-helix is necessary for its assembly. Subtle sequence variations within this highly conserved segment seem to determine whether or not a type IV pilin can be assembled into pili by the Pul secreton.

Introduction

The type II protein secretion (T2S) machinery, or secreton, of Gram-negative bacteria transports proteins from the periplasm across the outer membrane (Pugsley, 1993a; Sandkvist, 2001). It is composed of up to 14 different proteins, many of which share significant sequence similarities with components of the type IV pilus biogenesis pathway, also of Gram-negative bacteria (Pugsley, 1993a; Nunn, 1999; Sandkvist, 2001). The best-characterized component of both pathways is the secretin, an integral outer membrane protein that forms a multimeric channel complex (Bitter *et al*., 1998; Collins *et al*., 2001; 2003) through which the pilus (Wolfgang *et al*., 2000) or folded secreted proteins (Bitter *et al*., 1998; Brok *et al*., 1999; Nouwen *et al*., 1999; 2000) probably cross the outer membrane.

The 30 N-terminal amino acids of five secreton components, the pseudopilins, share substantial sequence similarity with the corresponding regions of type IV pilins (Pugsley, 1993a; Nunn, 1999; Sandkvist, 2001). This observation led to the idea that the pseudopilins might form a pilus-like structure (the pseudopilus) that functions either as a periplasmic scaffold on which other secreton components are assembled or as a piston-like motor to drive secretion across the outer membrane (Hobbs and Mattick, 1993; Pugsley, 1993a; Nunn, 1999; Sandkvist, 2001). Early studies with the pullulanase secreton from *Klebsiella oxytoca* failed to provide any evidence for such a pseudopilus, probably because only a small proportion of the pseudopilins are assembled at any given moment (Pugsley and Possot, 1993; Pugsley, 1996). The most abundant pseudopilin, PulG, was subsequently shown to assemble into long, bundled pili when expression of its structural gene was increased and the bacteria were grown on agar (Sauvonnet *et al*., 2000a; Pugsley *et al*., 2001; Vignon *et al*., 2003). These long pili were considered to result from the uncontrolled elongation of a normally shorter, periplasmic pseudopilus (Sauvonnet *et al*., 2000a; Vignon *et al*., 2003). This idea is supported by studies in *Xanthomonas campestris* showing that a PulG homologue, XpsG, forms intraperiplasmic complexes (Hu *et al*., 2002) and by the fact that similar phenomena have been reported for other T2S secretons (Durand *et al*., 2003; Vignon *et al*., 2003).

X-ray diffraction and NMR analyses of four full-length or N-terminally truncated type IV pilins (PilE from *Neisseria gonorrhoeae*, PilA from two strains of *Pseudomonas aeruginosa* and TcpA from *Vibrio cholerae*) revealed a considerable degree of structural conservation, despite the fact that major sequence similarities are restricted to the extreme N-terminal regions (Parge *et al*., 1995; Hazes *et al*., 2000; Keizer *et al*., 2001; Craig *et al*., 2003). The

Konstanzer Online-Publikations-System (KOPS)
URL: http://www.ub.uni-konstanz.de/kops/volltexte/2007/4053/
URN: http://nbn-resolving.de/urn:nbn:de:bsz:352-opus-40532

Table 1. *E. coli* strains.

Strain	Relevant characteristics	Source/reference
PAP105	*Δ(lac-proAB)* F′ *lacI*^{Q} Tn*10*	Laboratory collection
PAP7500BG	*araD139* (*argF-lac*)*U169 rpsL150 relA1 flbB5301 deoC1 ptsF25 malG501* F′ *lacI*^{q1} Tn*10 malP*::*(pulS pulA-pulB::kan1 pulCO)pulB::kan1* and Δ*pulG* (*pul* genes integrated into chromosome; lacks functional *pulG* gene)	Pugsley (1993b); Sauvonnet *et al*. (2000a)
PAP9001	*araD139* (*argF-lac*)*U169 rpsL150 relA1 flbB5301 deoC1 ptsF25 malE44 malG510 fimAB*::*kan sacB* (lacks type I pili)	Laboratory collection
PAP7501	PAP9001 F′ *lacI*^{Q} Tn*10*	Laboratory collection

conserved structural features include a long, N-terminal helix, the first, highly conserved part of which is hydrophobic, followed by loop structure and then several anti-parallel β-strands and a disulphide bridge near the C-terminus. The hydrophobic N-terminal helix is proposed to be required for pilin export across the plasma membrane, for retention of the unassembled pilin in this membrane and for the interactions that promote pilus assembly. Model building predicts that the pilins are arranged in a helical manner, with the hydrophobic N-terminal helix packed in the central core of the pilus, although the details of the models vary according to the particular pilin (Parge *et al*., 1995; Keizer *et al*., 2001; Craig *et al*., 2003; 2004).

Here we analyse the structure of PulG filaments by electron microscopy, present the structure of a truncated PulG determined by X-ray crystallography, and use this to build an atomic model. To gain further insight into pilus assembly and protein secretion, we analysed chimeric proteins formed by exchanging the N-terminal hydrophobic region between pseudopilins and pilins.

Results

Characterization of the PulG(His)^{6} helix

PulG(His)^{6} is identical to natural PulG except that the C-terminal sequence G^{132}K^{133}K^{134} (numbers refer to position in the mature PulG polypeptide chain) has been extended to G^{132}FHHHHHHK to incorporate a hexahistidine tag (Pugsley, 1993b). The protein is fully functional in secretion (Pugsley, 1993b) and forms pili when it is overproduced (Pugsley *et al*., 2001; Vignon *et al*., 2003). In contrast to pili formed by untagged PulG, pili formed by PulG(His)^{6} do not form bundles, which facilitates their analysis (Vignon *et al*., 2003).

PulG(His)^{6} pili were purified by shearing of agar-grown *Escherichia coli* K-12 PAP9001(pCHAP7009) (see Tables 1 and 2 for details of strains and plasmids) and cobalt affinity chromatography essentially as described previously (Vignon *et al*., 2003). The strain used here lacks the *pulA* gene coding for the secreted enzyme pullulanase that contaminated earlier samples of PulG(His)^{6}

Table 2. Plasmids.

Plasmid	Vector/replication origin/ resistance	Cloned genes and/or chimeras	Reference and/or source of cloned fragment
pCHAP231	pBR322/pColE1/Ap	pBR322::(*pulS pulA-B pulC-O*)	d'Enfert *et al*. (1987)
pCHAP1216	pBR322/pColE1/Ap	pCHAP231 *pulB::kan-1ΔpulG*	Possot *et al*. (2000)
pCHAP1362	pSU19/p15/Cm	*lacZ*p-*pulG::His*^{6}	Pugsley (1993b)
pCHAP3100	pSU18/p15/Cm	*lacZ*p-*ppdD*	Sauvonnet *et al*. (2000a)
pCHAP1379	pSU18/p15/Cm	*lacZ*p-*pilA*	This study
pCHAP1404	pSU18/p15/Cm	*lacZ*p-*pilE*	This study
pCHAP1418	pSU19/p15/Cm	*lacZ*p-*tcpA*	This study
pCHAP4260	pUC18/pColE1/Ap	*lacZ-pelB′*	O. Francetic
pCHAP7003	pSU19/p15/Cm	*lacZ*p-*ppdD, pulG::His*^{6}	This study
pCHAP7007	pUC19/pColE1/Ap	*pulB*::*kan-1-pulF*	This study
pCHAP7008	pUC19/pColE1/Ap	*pulB*::*kan-1-ΔpulA-pulF*	This study
pCHAP7009	pBR322/pColE1/Ap	pCHAP231 *pulB*::*kan-1ΔpulG,ΔpulA*	This study
pCHAP7010	pUC18/pColE1/Ap	*pelBss::pulG(25-134)::His*^{6}	This study
pCHAP7012	pSU18/p15/Cm	*pelBss::pulG(25-134)::His*^{6}	This study
pCHAP7013	pT7-5/PColE1/Ap	T7p-*pelBss::pulG(25-134)::His*^{6}	This study
pCHAP7015	pSU18/p15/Cm	*lacZ*p-(*ppdD17::pulG::His*^{6})	This study
pCHAP7016	pSU18/p15/Cm	*lacZ*p-(*pilE17::pulG::His*^{6})	This study
pCHAP7017	pSU18/p15/Cm	*lacZ*p-(*pulG17::pilE*)	This study
pCHAP7019	pSU18/p15/Cm	*lacZ*p-(*pulG21::ppdD*)	This study
pCHAP7023	pSU18/p15/Cm	*lacZ*p-(*pulG17::ppdD*)	This study
pCHAP7024	pSU18/p15/Cm	*lacZ*p-(*ppdD21::pulG::His*^{6})	This study
pCHAP7026	pSU18/p15/Cm	*lacZ*p-(*pulG17::pilA*)	This study
pCHAP7027	pSU18/p15/Cm	*lacZ*p-(*ppdD21::pilA*)	This study

Ap, ampicillin; Cm, chloramphenicol.

pili (Vignon *et al*., 2003). Images of uranyl acetate stained PulG(His)^6 pili recorded in a scanning transmission electron microscope (STEM) revealed mainly long filaments with pronounced flexibility (Fig. 1A). Distinct repeating protrusions, suggestive of a helical structure, became visible at higher magnification (Fig. 1B). Although the negative stain penetrated deeply into the grooves between the protrusions, there was no indication of a central, stain-filled cavity. The handedness of the pilus helix was determined by metal shadowing experiments, which revealed a left-handed twist (Fig. 1C).

Twenty-seven negatively stained PulG(His)^6 pili in the STEM images were analysed for structural information. Selected segments were first computationally straightened (Fig. 2A) and the average profile perpendicular to the filament axis was calculated to determine their outer diameter (8.2 ± 0.3 nm). The full-width-half-maximum (FWHM) diameter measured on freeze-dried, unstained filaments was 6.9 ± 1.0 nm (see below). Most diffraction patterns from straightened rods exhibited the *x*-pattern typical of helical symmetry (Fig. 2B) but many were not symmetrical with respect to the meridian, indicating uneven staining and unsatisfactory structural preservation. The strongest layer lines of all 27 filaments were $(4.38 \pm 0.12\ \text{nm})^{-1}$ from the equator, reflecting the pitch of the genetic helix (i.e. the lowest pitch one-start helix describing the helical symmetry of the structure; see DeRosier and Klug, 1968). Amplitude and phase plots of this layer line calculated from the pilus segment shown in Fig. 2A exhibit a minor asymmetry in the amplitude (Fig. 2C) and a phase difference of π between the left and right side (Fig. 2D). Because the distance between the major maxima corresponded to $(5.4\ \text{nm})^{-1}$, and the filament radius was 3.5–4.1 nm, this layer line is best described by a first-order Bessel function (J_1), suggesting that the pilus is a one-start helix.

In an attempt to identify the helical repeat, PulG(His)^6 pilus stretches of up to 157 nm length were examined using a 'linear Markham' superposition algorithm (Hahn *et al*., 2000). Repeat lengths, ranging from 7 pixels up to the largest possible were tested (i.e. 238 pixels, 78 nm, for the longest pilus when two stretches were averaged). The enhancement resulting from superposition and averaging was quantified by comparing the root mean square (rms) deviation of the average with that of the unprocessed segment. Plots of the rms quotient against the repeat length exhibited series of maxima for all 27 pili. The repeats were 4.37 ± 0.85 nm apart for the six best-preserved pilus rods. This separation corresponds to the pitch of the genetic helix, in good agreement with the position of the prominent layer line in Fig. 2B. Averaging the Markham superposition curves for 7 well-preserved pili yielded a distinct maximum of the rms quotient at 17.5 nm, the peak height of which is more than 10%

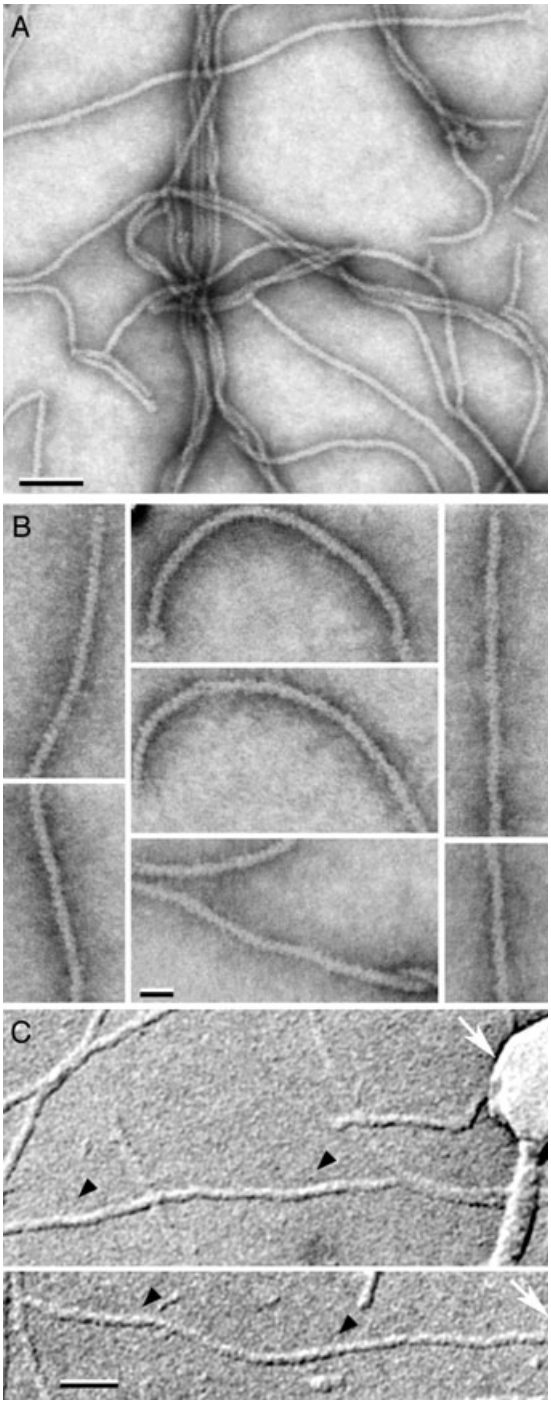

Fig. 1. Appearance of the PulG(His)^6 pili.
A and B. Negatively stained pili imaged by the STEM. (A) Single and intertwined twisting pili. (B) The periodic helical structure is distinct at higher magnification, even in the bent regions of PulG(His)^6 pili. A stained filled central cavity could not be detected.
C. PulG(His)^6 pili imaged by transmission electron microscope after shadowing with W/Ta. A left-handed helical twist is clearly visible when viewing at a glancing angle in the direction indicated by black arrows. The T4 phage tail also present displays the expected right-handed helical symmetry. The direction of shadowing is indicated (white arrow).
Scale bars: 50 nm in (A) and (C), 20 nm in (B).

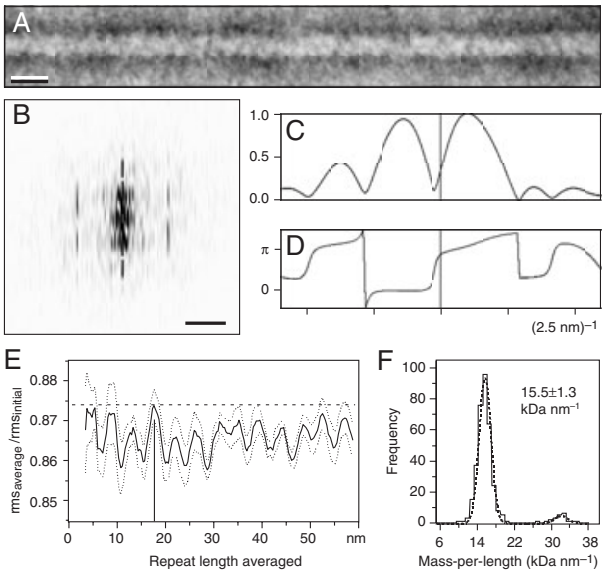

Fig. 2. Analysis of straightened pilus stretches.
A. Distinct regular peripheral projections indicate the helical architecture (scale bar 10 nm).
B. The diffraction pattern reveals the characteristic *x*-pattern for a helical structure, with the strong layer line at $(4.37\ \text{nm})^{-1}$.
C and D. Amplitude (C) and phase plots (D) of the strong layer line indicate a first-order Bessel function (see text).
E. Markham superposition yields a regular repeat of 4.38 nm, corresponding to the pitch of the genetic helix. The plot shown is the average (solid line) from seven pili, with dotted lines marking the standard error. The peak at 17.5 nm stands out and indicates that the pili have four turns per helical repeat.
F. The mass-per-length histogram comprises measurements of 331 pilus stretches of ≈ 80 nm length.
Scale bars: 10 nm in (A) and 5 nm in (B).

above all of the other maxima, disregarding the first rather noisy maximum of almost equal height (Fig. 2E). Thus, the helical repeat of the PulG(His)^6 pilus appears to contain four turns.

To establish the number of subunits per helical repeat, a series of low-dose dark-field images was recorded from freeze-dried, unstained PulG(His)^6 samples by STEM, and the mass-per-length (MPL) of the PulG(His)^6 rods determined (Müller *et al.*, 1992). The pooled MPL data from 331 pilus segments yielded a histogram that is described by a single Gauss curve peaking at 15.5 ± 1.3 kDa nm^{-1} after correction for mass loss [standard error (SE) = ±0.07 kDa nm^{-1}; Fig. 2F]. The overall uncertainty of the measurement is ±0.8 kDa nm^{-1} considering the SE of the result and the 5% calibration uncertainty of the microscope. The average FWHM diameter of the unstained PulG(His)^6 pili (see above) was 6.9 ± 1.0 nm (see *Experimental procedures*). Because the PulG(His)^6 pili are homopolymers of the 15.4 kDa protein PulG(His)^6 (Pugsley, 1993b), the number of protein monomers per helical repeat can be directly calculated from the MPL. Accordingly, 17.64 ± 0.92 subunits would assemble into a full helical repeat comprising four helical turns.

Taking together the layer line analysis, which suggests the PulG(His)^6 pilus to be single started, the MPL and Markham superposition results, a compatible helical selection rule is $l = 4n + 17m$, where l is the layer line number ($l = 0, \pm1, \pm2 \ldots$), m the meridian branch number ($m = 0, \pm1, \pm2 \ldots$) and n the Bessel order sampled on layer line l ($n = 0, \pm1, \pm2 \ldots$). Several helical selection rules were explored because the PulG(His)^6 pili exhibited pronounced flexibility. The simplest rules delineating the range tested were $l = 1n + 4m$ ($\psi = 90°$) and $l = 1n + 5m$ ($\psi = 72°$), where the screw angle ψ is the angle by which adjacent subunits are rotated relative to each other. To sample this screw angle interval (i.e. 72°–90°), all 33 helical selection rules from 1*n* to 10*n* with screw angles between 72° and 90° were applied to the 14 best PulG(His)^6 pili. Their two-dimensional (2D) Fourier transforms were calculated and the power transmitted (PT) by the $D(Z,k)$ filter derived from the respective helical selection rule was determined (Smith and Aebi, 1974). The PT was smaller for the longest helical repeats (9*n* and 10*n*) than for the shorter helical repeats (4*n*, 6*n*, 7*n* and 8*n*) over the entire screw angle range tested, indicating variations of the helical structure along the rod axis. All helical selection rules explored having screw angles between 80° and 90° yielded higher PT values than those between 72° and 80°, with a global flat maximum around 85°. This maximum is within the restriction dictated by the MPL value (15.5 ± 0.8 kDa nm^{-1}), which limits the range of screw angles to 83°–86°.

As a result of their inherent flexibility (see Fig. 1), the best helical selection rule describing the PulG(His)^6 pili varied depending on the pilus stretch tested, the variation complying to the screw angle range 83°–86°. Accordingly, the pilus structure should be described by the rule that corresponds to the average situation, i.e. to a screw angle of ≈ 84.5°. This requirement is met by the rule $l = 4n + 17m$ ($\psi = 84.7°$), which was accordingly used to $D(Z,k)$-filter the Fourier transform of the pilus shown in Fig. 2A. The three-dimensional (3D) helical reconstruction was then produced from the filtered layer lines 0 to ±8, including 12 Bessel orders, which corresponds to a resolution of $(2.3\ \text{nm})^{-1}$. A 3D map thus reconstructed from the negatively stained PulG(His)^6 pilus was isocontoured to include 100% of the mass (see *Experimental procedures*). This envelope served as a guide to build an atomic model of the PulG(His)^6 pilus (see below).

Construction and purification of a soluble, truncated PulG variant for structural analysis

Attempts to crystallize full-length PulG(His)^6 obtained by dissociating purified pili in the detergent C_8E_4 failed. The

N-terminal hydrophobic region was therefore deleted by fusing the C-terminal hydrophilic domain (from position +25 relative to the prepeptide cleavage site) to the *Erwinia chrysanthemi* pectate lyase PelB signal peptide ($PelB^{SP}$). This strategy was judged appropriate because studies with type IV pilins from *P. aeruginosa* indicate that truncation at the N-terminus of the pilin monomer does not affect its structure (Hazes *et al*., 2000; Keizer *et al*., 2001; Craig *et al*., 2003). In *E. coli*, the truncated PulG variant was abundant and readily released by osmotic shock, suggesting that the signal peptide is efficiently processed by leader peptidase. When produced in cells expressing a complete set of *pul* genes (pCHAP231), $PelB^{SP}$-$PulG_{25\text{-}134}(His)^6$ interfered with neither pullulanase secretion nor PulG pilus assembly (data not shown). $PelB^{SP}$-$PulG_{25\text{-}134}(His)^6$ did not restore pullulanase secretion or piliation in strains lacking PulG, in line with previous results obtained with a poorly expressed and poorly processed $MalE^{SP}$-PulG construct (Pugsley, 1996).

$PulG_{25\text{-}134}(His)^6$ was extracted and purified from the periplasm (see *Experimental procedures*). N-terminal sequence analysis indicated precise cleavage by signal peptidase. $PulG_{25\text{-}134}(His)^6$ eluted close to the size predicted for a monomer upon gel filtration in the presence (Fig. 3) or absence (not shown) of 0.7% C_8E_4, indicating that PulG can not multimerize efficiently without its N-terminal hydrophobic domain. In contrast, full-length $PulG(His)^6$ in the same detergent eluted as a multimeric complex (possibly a dimer) when examined by gel filtration (Fig. 3) and formed aggregates when the detergent was removed. The position of the peaks in these experiments was unaffected by the amount of material loaded on the column (not shown). Dynamic light scattering experiments gave mass estimates of 14 kDa for $PulG_{25\text{-}134}(His)^6$ and 42 kDa for full-length $PulG(His)^6$ in C_8E_4 (assuming that the molecules are close to spherical), which are somewhat lower than the estimates given by the gel filtration data in Fig. 3 (not shown).

Crystallization and structure determination of the C-terminal PulG domain

Purified $PulG_{25\text{-}134}(His)^6$ and a selenomethionine derivative were crystallized as described in *Experimental procedures*. $PulG_{25\text{-}134}(His)^6$ crystals diffracted to better than 1.6 Å (see Table 3). Experimental phases obtained from the selenomethionine derivative yielded an electron density map into which the model of $PulG_{25\text{-}134}(His)^6$ was built and refined against the 1.6 Å native data to a final R-factor of 16.6% (R_{free} = 19.9%). The atomic model comprises two chains each consisting of 108-amino-acid residues that represent a dimer in the asymmetric unit. The N-terminal methionine and the last eight amino acids, including the $(His)^6$ tag, were not visible in the electron density. Model statistics are listed in Table 4.

In contrast to its behaviour in aqueous solution (see above), $PulG_{25\text{-}134}(His)^6$ forms an apparently stable dimer under the crystallization conditions (Fig. 4). Each monomer consists of an extended N-terminal α-helix (amino acids 27–54) that is followed by a 44-amino-acid-long loop region (amino acids 54–98) containing a 3_{10}-helix (amino acids 64–67) and a C-terminal anti-parallel β-sheet (amino acids 99–128). Whereas the β-strands S1–S3 (amino acids 99–101; 110–113; 121–123) are consecutively arranged around the α-helix, β-strand S4 (amino acids 126–128) sticks out of the globular domain and interacts with β-strand S3 of the other monomer in the asymmetric unit. This strand exchange results in an intermolecular four-stranded, anti-parallel β-sheet. The nine-amino-acid-long loop region between β-strands S1 and S2 is stabilized by a second 3_{10}-helix (amino acids 105–107) of exactly one turn.

Even though metals were not added to the crystallization mixture, the crystal structure contains a metal ion on the non-crystallographic twofold axis and completely buried by the two PulG monomers. The tetrahedral coordination is maintained by one oxygen of the carboxylic

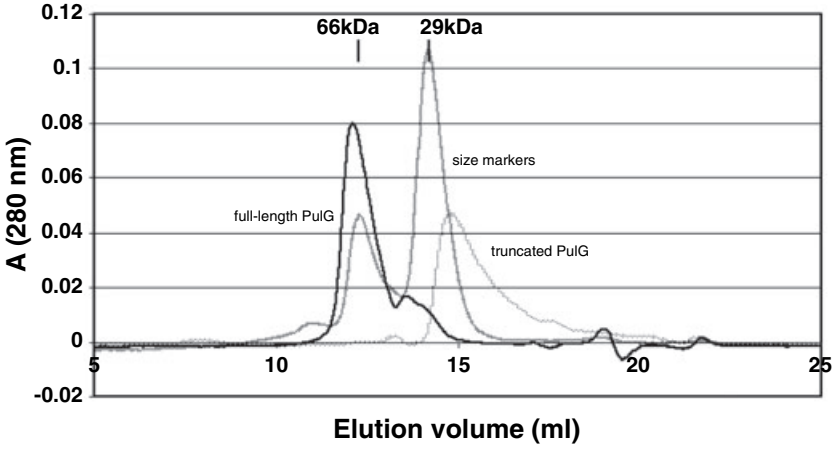

Fig. 3. Gel filtration of detergent solubilized, affinity-purified, full-length $PulG(His)^6$ and $PulG_{25\text{-}134}(His)^6$ (i.e. truncated PulG) on a Superose12 column (Pharmacia). $PulG(His)^6$ eluted at ≈ 66 kDa that includes a C_8E_4 micelle of about ≈ 17 kDa, whereas $PulG_{25\text{-}134}(His)^6$ eluted at ≈ 20 kDa.
A, absorbance.

Table 3. Crystallography data and refinement statistics.

Data set	Native rotating anode	Native synchrotron	Native merged	Se[a] remote high	Se[a] inflection point
Wavelength (Å)	1.54179	0.91964		0.97857	0.97972
Space group	$P6_522$	$P6_522$	$P6_522$	$P6_522$	$P6_522$
Cell a, c (Å)	85.31, 145.67	85.48, 145.78	85.40, 145.73	84.93, 144.19	84.40, 143.07
Resolution (Å)	50.00–1.95 (2.00–1.95)	50.00–1.60 (1.65–1.60)	50.00–1.60 (1.65–1.60)	50.00–2.80 (2.90–2.80)	50.00–2.80 (2.90–2.80)
Observed reflections	699 670 (50 178)	314 459 (31 263)	1 018 973 (31 263)	110 857 (10 440)	110 456 (10 111)
Unique reflections	23 399 (1670)	38 703 (3634)	40 533 (3634)	14 354 (1462)	14 353 (1462)
Completeness (%)	99.8 (99.3)	91.9 (99.7)	96.2 (99.7)	100 (100)	100 (100)
Wilson B-factor (Å^2)	29.9	27.8	29.0	29.2	25.0
I/σ(I)	27.0 (7.5)	14.2 (4.2)	19.1 (4.1)	24.0 (11.9)	20.8 (7.5)
R_{sym} (%)	11.1 (55.7)	7.5 (51.7)	12.8 (52.0)	6.9 (16.8)	8.5 (25.1)
R_{meas}[b] (%)	11.3 (56.7)	8.1 (55.0)	13.0 (55.3)	7.4 (18.2)	9.1 (27.1)
$R_{mrgd\text{-}F}$[b] (%)	4.5 (12.2)	6.2 (25.7)	5.8 (26.2)	3.6 (9.0)	5.0 (15.5)

a. Crystal with selenomethionine substitution.
b. Defined by Diederichs and Karplus (1997).
Values in parentheses correspond to the highest resolution shells.

side-chain of E44, one water and their twofold partners in the middle of the N-terminal α-helices. Residue N123 at the end of β-strand S3 and its twofold partner additionally stabilize the metal binding site by hydrogen bonds from their δ-oxygens to the non-coordinating oxygens of E44 and from their δ-nitrogens to the coordinating water molecules (Fig. S1). For reasons explained in *Supplementary material*, this metal ion was tentatively identified as Zinc, probably derived from the buffers used in the crystallization.

The dimer interface

Both PulG monomers in the asymmetric unit form a compact, apparently stable structure. Several factors are involved in the tight protein–protein interactions and play an important role in dimerization:

i. tight side-chain interactions between the N-terminal α-helices of the two monomers,
ii. the coordination of a metal ion (probably zinc) to the carboxyl oxygen of each E44 residue,
iii. two intermolecular salt bridges, one on each side of the two long helices between residues K30 and D53 and
iv. the strand exchange between the S4 β-strands, which sequesters hydrophobic residues of the S3-S4 loop from water.

Table 4. Crystallographic refinement statistics.

Resolution range (Å)	50.0–1.6 (1.64–1.60)
No. of reflections total	40533 (3046)
No. of reflections for R_{free} calculation	2037 (152)
R, R_{free} values (%)	16.8, 19.9 (20.3, 22.0)
Molecules/asymmetric unit	2
Solvent content (%)	59
No. of protein atoms	1686
No. of solvent waters	257
No. of metal ions	1
Mean B-factor, protein atoms (Å^2)	27.4
Mean B-factor, solvent atoms (Å^2)	42.8
B-factor, zinc ion (Å^2)	20.9
Ramachandran plot[a]	
Most favoured regions (%)	92.4
Additional allowed regions (%)	7.6
Generously allowed or disallowed regions (%)	0.0
rms. deviation bond length (Å)	0.012
rms. deviation bond angle (°)	1.42

a. Given by PROCHECK (Laskowski *et al.*, 1993).
Values in parentheses correspond to the highest resolution shells.

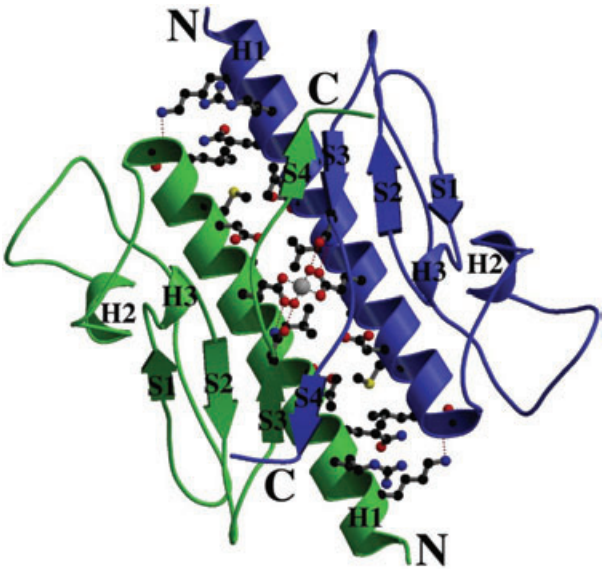

Fig. 4. Structure of a $PulG_{25\text{-}134}(His)^6$ dimer (pdb code ITa2). Each monomer consists of a long N-terminal α-helix (H1) followed by an extended loop region containing a 3_{10}-helix (H2) and a C-terminal four-stranded β-sheet (S1–S4). Another 3_{10}-helix (H3) is found in the loop connecting S3 and S4. The tetrahedrally coordinated metal ion on the centre of the non-crystallographic symmetry axis was modelled as a zinc atom. Dashed black lines represent the coordinating atoms. Salt bridges on both sides of the two helices between K30 and D53 are shown as dashed red lines. The residues of the N-terminal helices of both monomers that account for most of the contact area are shown in a ball and stick representation.

The net result is a large contact area of 1094 Å^2 (calculated with GRASP; Nicholls *et al*., 1991) that is buried between both monomers. Most residues in the contact area are contributed by the N-terminal helices and by β-strands S3 and S4.

Comparison of the PulG structure with those of type IV pilins

Type IV pilins are grouped into type IVa and type IVb according to the length of the prepeptide that is removed by prepilin peptidase (Peabody *et al*., 2003). They all share a common arrangement of the major secondary structure elements that form a core structure consisting of an extended N-terminal α-helix and a four-stranded anti-parallel β-sheet (Fig. 5). These features are also present in PulG (Fig. 5) (see *Discussion*).

Model of the PulG(His)^6 pilus helix and assessment

The combination of the atomic PulG structure, the modelling of the PulG N-terminal α-helix hydrophobic extension (*Experimental procedures*) and the extensive filament analysis, including the information from the metal shadowing experiments, enabled a model of the helical arrangement to be built (Fig. 6; see *Experimental procedures*). Compact packing of the centrally oriented hydrophobic α-helices of the left-handed filament ensures stability. Prominent bulges occur along its surface, reflecting this distinct feature of the negatively stained pili as well as the left-handed helical groove of metal-shadowed filaments (Fig. 1). In contrast, a right-handed filament model built to test the data (not shown) had a smoother surface and the monomers were packed more tightly along the axis, making the helical groove less distinct. These features would probably make the right-handed variant less flexible than the left-handed one, which would be incompatible with the bent PulG(His)^6 pili observed by STEM analysis (Fig. 1).

Influence of the N-terminal helix and the head domain on the assembly of type IV pilins by the Pul secreton

The structural analyses reported above revealed that the PulG pili probably have the same overall structural organization as type IV pili. The Pul secreton can assemble several different PulG homologues into pili (Vignon *et al*., 2003), suggesting that the assembly machinery is rather promiscuous. The *E. coli* K-12 type IV pilin PpdD can also be assembled into bundled pili by the Pul secreton in *E. coli* but can not substitute for PulG in pullulanase secretion (Sauvonnet *et al*., 2000a). However, none of three other type IV pilins tested, PilA (*P. aeruginosa* PAK; pCHAP1379; referred to hereafter as PilA^{PAK}), PilE [*N. gonorrhoeae* N400 (MS11); pCHAP1404] and TcpA (*V. cholerae*, pCHAP1418), was assembled into pili by the Pul secreton in *E. coli* carrying pCHAP1216 (*pul* secreton

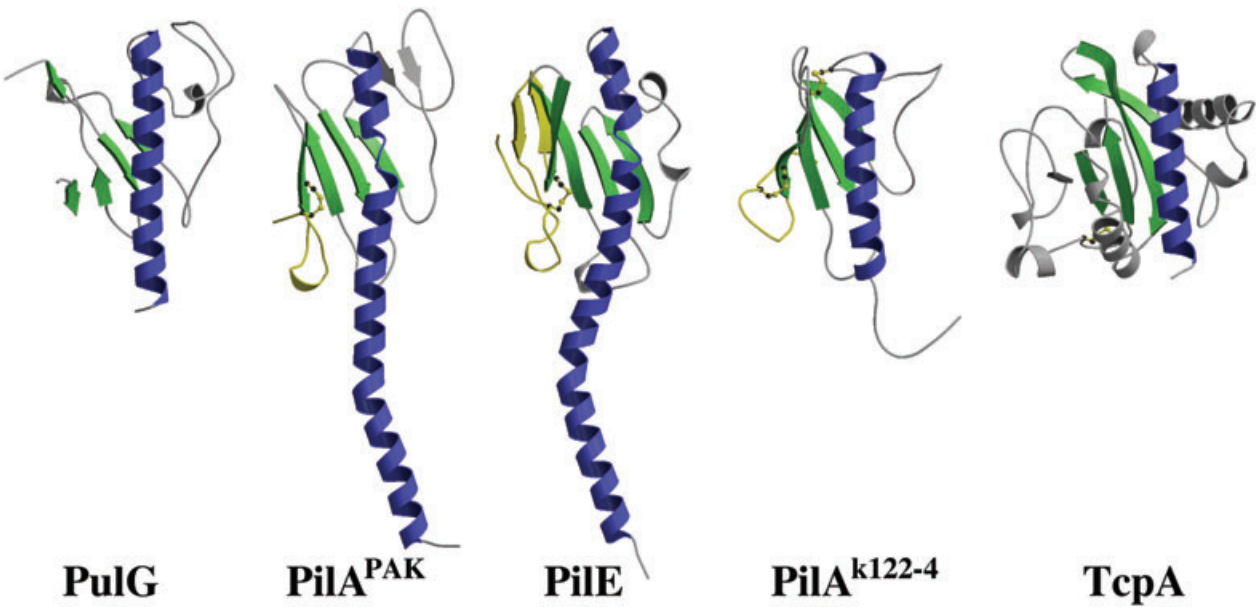

Fig. 5. Comparison of the crystal structure of a PulG$_{25-134}$(His)^6 monomer with known structures from the type IVa pilins PilA from *P. aeruginosa* strain PAK (pdb code 1OQW), PilE from *N. gonorrhoeae* strain MS11 (pdb code 2PIL), PilA from *P. aeruginosa* strain k122-4 (pdb code 1HPW) and the type IVb pilin TcpA from *V. cholerae* (pdb cade 1OQV). To facilitate comparison, all structures are shown in the same orientation and the PulG β-strand S4 from the other monomer is also shown because this is the putative conformation in the monomeric form. Secondary structure elements correspond to the definition of DSSP (Kabsch and Sander, 1983) with one exception: β-strand S4 of PilA^{k122-4} did not fulfil the strict criteria of DSSP but was clearly visible as a slightly distorted β-strand and is included in the figure.

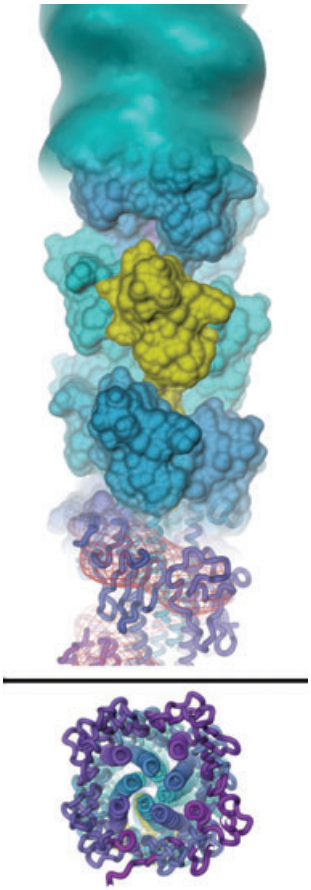

Fig. 6. Atomic model of the PulG pilus. A left-handed model was based on the average helical selection rule $4n + 17m$ derived from the microscopic analysis of PulG pili (see Fig. 2). The figure shows the envelope of the helical reconstruction of the pilus at 2.5 nm resolution, the arrangement of the PulG monomers and the interaction of the N-terminal helices (from top to bottom). Views up along the pilus axis are displayed at the bottom.

genes in pBR322 derivative with a Δ*pulG* mutation), despite correct processing by prepilin peptidase PulO (Dupuy *et al*., 1992; Fig. S2) (data not shown).

N-terminal hydrophobic regions of type IV pilins/pseudopilins are likely to be a key factor in both subunit recognition by the assembly machinery and subunit interactions in the pilus. Differences in these regions could therefore explain the failure of the Pul secreton to assemble PilA, PilE and TcpA. The sequences of these regions are highly conserved but the fact that they are missing from most known pilin/pseudopilin structures, including that of PulG, makes direct comparisons difficult. Homology analysis (http://www.fundp.ac.be/sciences/biologie/bms/matchbox_submit.html) revealed that the first 23 amino acids of $PilA^{PAK}$ and PilE are very similar to those of PulG, whereas the corresponding sequence of PpdD is more distantly related, and that of the type IVb group pilin TcpA shares the lowest degree of similarity with that of PulG (see *Supplementary material*). Therefore, a series of chimeras was constructed to test the role of the N-terminal hydrophobic helix in the failure of the Pul secreton to assemble some type IV pilins.

Because PpdD is assembled by the Pul secreton, 17-, 21- and 26-amino-acid N-terminal segments of PulG and PpdD were exchanged. For simplicity, these chimeras are called G_{17}-D, G_{21}-D, G_{26}-D, D_{17}-$G(His)^6$, D_{21}-$G(His)^6$ and D_{26}-$G(His)^6$, where the letters G and D refer to PulG and PpdD, respectively, and the numbers indicate the amino acids present, counting from position +1. The G_{26}-D and D_{26}-$G(His)^6$ chimeras could not be detected by immunoblotting of whole-cell lysates, suggesting that they are rapidly degraded, and were not examined further. The results obtained with these and other chimeras are summarized in Table 5.

G_{17}-D (pCHAP7023) and G_{21}-D (pCHAP7019) were not found in more than trace amounts in the sheared (released pilus) fractions of *E. coli* cells in which the secreton genes (except *pulG*) were in the chromosome or on pCHAP1216 (see Table 2), even though the proteins were at least as abundant as PpdD, which was efficiently assembled in the control cells expressing unmodified *ppdD* (Fig. S3). These results were confirmed by immunoelectron microscopy (EM), which failed to reveal the presence of any pili on the surface of bacteria expressing these chimeras (data not shown). Site-directed mutagenesis failed to identify any particular residues in the PulG-derived part of G_{21}-D that were responsible for its failure to assemble into pili (see *Supplementary material* and Figs S4 and S5).

In contrast, the reciprocal chimera D_{17}-$G(His)^6$ (pCHAP7015) was assembled into pili, as revealed by shearing and immuno-EM analyses (Fig. 7A, lanes 1 and 2, Fig. 7B and Table 5) and was functional in secretion (data not shown). The additional exchange of four amino acids, generating the chimera D_{21}-$G(His)^6$ (pCHAP7024), abolished piliation and secretion (Fig. 7A, lanes 3 and 4, and data not shown).

Chimeras in which the first 17 amino acids of $PulG(His)^6$ and PilE were exchanged were then constructed. The resulting hybrids [G_{17}-E (pCHAP7017) and E_{17}-$G(His)^6$ pCHAP7016)] were stable and were found in the sheared fraction (Table 5; Fig. 8A, lanes 4–8, Fig. 8B and C). The amount of G_{17}-E in the sheared fraction was very low and could be explained by the release of membrane material (note the contamination of the sheared fraction by outer membrane protein LamB in Fig. 8A, lane 6). Therefore, these bacteria were also examined by immuno-EM. While the E_{17}-$G(His)^6$ pili appeared normal (Fig. 8B), the G_{17}-E pili were abnormally thick, although they were clearly able to react with the PilE antibodies (Fig. 8C). As expected, only E_{17}-$G(His)^6$ was functional in secretion (not shown).

Because G_{17}-E could be assembled by the Pul secreton, chimeras between PulG and $PilA^{PAK}$ were constructed

Table 5. Assembly of PulG type IV pilin chimeras by the Pul secreton of *K. oxytoca* in *E. coli* and their ability to promote pullulanase secretion.

Protein	N-terminal region	C-terminal region	Junction (amino acid)	Assembly	Pullulanase secretion
PulG(His)^6	PulG	PulG(His)^6	na	+	+
PppD	PpdD	PpdD	na	+	–
G_{17}-D	PulG	PpdD	17–18	–	–
G_{21}-D	PulG	PpdD	21–22	–	–
D_{17}-G(His)^6	PpdD	PulG(His)^6	17–18	+	+
D_{21}-G(His)^6	PpdD	PulG(His)^6	21–22	–	–
PilE	PilE	PilE	na	–	–
G_{17}-E	PulG	PilE	17–18	(+)[a]	–
E_{17}-G(His)^6	PilE	PulG(His)^6	17–18	+	+
PilA^{PAK}	PilA^{PAK}	PilA^{PAK}	na	–	–
G_{17}-A	PulG	PilA^{PAK}	17–18	–	–
G_{21}-A	PulG	PilA^{PAK}	21–22	+	–

a. Deformed pili observed by electron microscopy; see text.
na, not applicable.

[G_{17}-A^{PAK} (pCHAP7026) and G_{21}-A^{PAK} (pCHAP7027)] (Table 5). G_{21}-A^{PAK} but not G_{17}-A^{PAK} was found in the concentrated sheared fraction (Fig. 9A). Although the amount of G_{21}-A^{PAK} detected in the sheared fraction was even lower than with PilA itself (lane 2), the majority of the cells producing this chimera possessed one or a limited number of often deformed or abnormal pili (Fig. 9B).

Taken together, these results indicate that the authentic type IV pilins PilE and PilA^{PAK} can be assembled into pili by the Pul secreton when fused to the first 17 or 21 amino acids, respectively, of the hydrophobic domain of wild-type PulG but the assembly efficiency was never as good as with PulG or PpdD. Thus, despite their considerable similarity, the N-terminal regions of pseudopilins and pilins can not be considered as fully interchangeable (see *Discussion*).

A type IV pilin is not assembled into PulG-containing pili

We showed previously that PulG and PpdD can be assembled into the same pilus bundles but it was not clear whether PpdD actually formed separate pili or was co-assembled into pili containing PulG (Sauvonnet *et al.*, 2000a). The discovery that a His tag at the C-terminal end of PulG prevented bundle formation without affecting pilus formation and facilitated pilus purification (Vignon *et al.*, 2003) allowed this issue to be addressed.

Pili formed when PpdD and PulG(His)^6 were co-produced in cells carrying pCHAP7003 [tandem copies of *ppdD* and *pulG*(*His*)^6] and lacking the *lacI*^{q1} repressor gene were purified by cobalt affinity chromatography (Vignon *et al.*, 2003). Both PpdD and PulG(His)^6 were found in the sheared fraction (Fig. 10A, lanes 2 and 6). Most of the PulG(His)^6 in the sheared fraction bound to the resin and eluted with imidazole (Fig. 10A, lane 4) but only trace amounts of PpdD were retained (lane 8), the majority being present in the flow-though fraction (lane 7), indicating that very little PpdD was present in the PulG(His)^6 pili. This conclusion was confirmed by double labelling immuno-EM studies that revealed PpdD exclusively in clusters or blebs that were sometimes attached to the pili, which were uniformly labelled by anti-PulG (Fig. 10B). Therefore, non-specific co-purification of the attached PpdD clusters probably explains the small amount of PpdD that binds together with PulG(His)^6 to the cobalt resin. Thus, assembly of PpdD into pili seems to be prevented by the assembly of PulG.

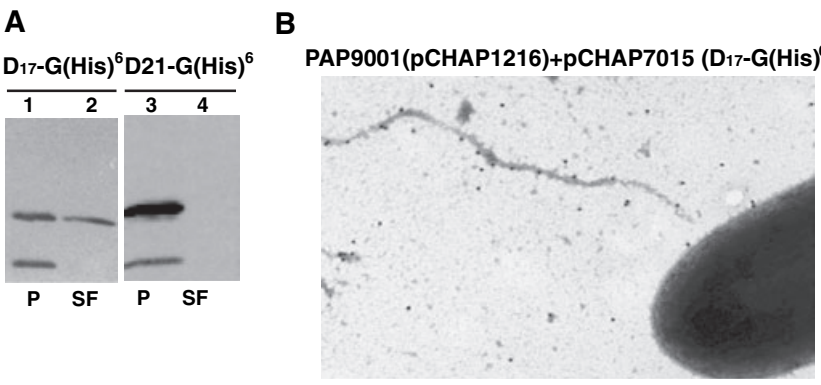

Fig. 7. A. Immunoblotting of pellet (P) and shearing fractions (SF) of PAP9001(pCHAP1216) carrying pCHAP7015(D17-G(His^6)) or pCHAP7024(D21-G(His^6)).
B. Immuno-EM of PAP9001(pCHAP1216) + pCHAP7015(D17-G(His^6)) in which pili were labelled with anti-PulG antibodies, followed by secondary antibodies coupled to 5 nm gold beads.

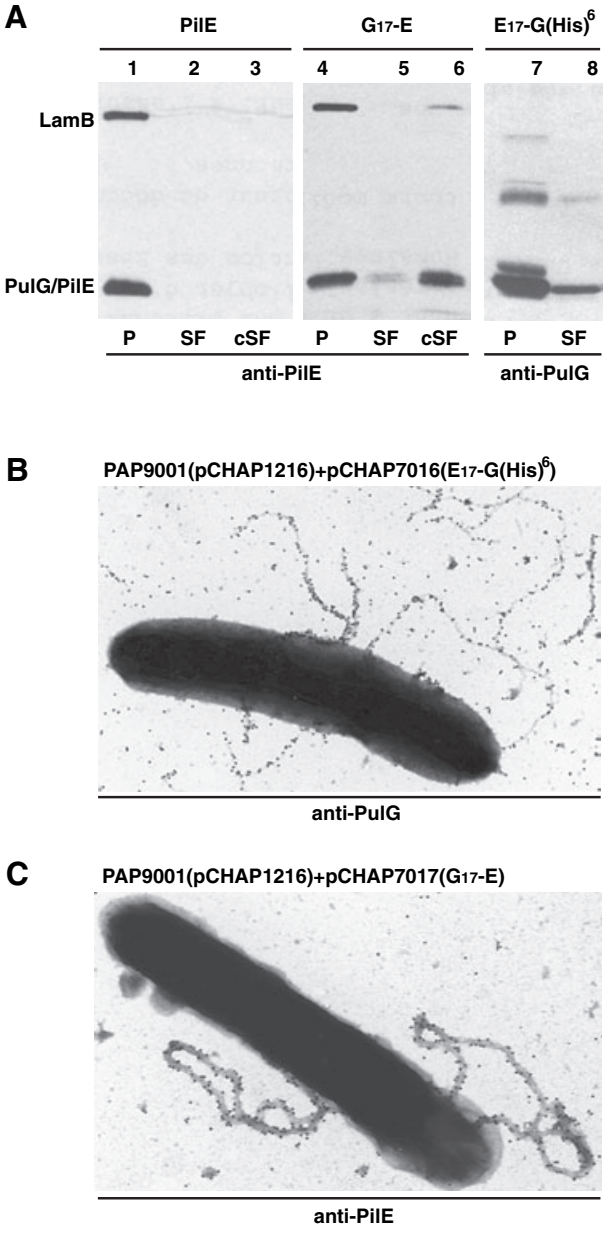

Fig. 8. A. Analysis of pellet and shearing fractions by immunoblotting of PAP9001(pCHAP1216) transformed with pCHAP1404(PilE), pCHAP7017(G_{17}-E) and pCHAP7016(E_{17}-G(His)^6) respectively. Blot membranes were probed with anti-PilE or anti-PulG antibodies. Antibodies against outer membrane protein LamB were used to assess the release of membrane fragments. P, pellet fraction after shearing; SF, sheared fraction; cSF, concentrated sheared fraction.
B and C. Immuno-EM of PAP9001(pCHAP1216) harbouring pCHAP7016(E_{17}-G(His^6)) (B) and pCHAP7017(G_{17}-E) (C), respectively, labelled with anti-PulG or anti-PilE antibodies, followed by secondary antibodies coupled to 5 nm gold beads.

Discussion

The crystal structure reported here confirms the long-suspected structural similarity between the pseudopilin PulG and type IV pilins. Despite the lack of substantial sequence similarity (other than the first half of the long N-terminal α-helix), PulG and the type IVa pilins display a similar overall structural organization, comprising the long α-helix followed by four anti-parallel β-strands. Nevertheless, PulG is more compact than type IVa pilins, and much more compact than the larger type IVb pilin TcpA (Fig. 5). The conformation of the loop regions is conserved neither between the pilins and the pseudopilin nor within the IVa pilins. TcpA, the only type IVb pilin whose structure is known, shows a different fold because the β-strands of the core structure have another arrangement. Despite the marked differences between PulG and TcpA, structure-based alignments show that these two proteins share 16 identical residues on superposition using a 5 Å cut-off, compared with only eight for PilE and PulG and four for PilA and PulG (see *Supplementary material*, Table S1 and Fig. S6 for further information).

PulG lacks the loop region between the two cysteine residues that are conserved in all type IV pilins. The sequence of this region of type IV pilins is extremely variable, even in closely related pilins from the same species of bacteria, and represents a major epitope that is exposed on the surface of the pilus (Hagblom *et al.*, 1985). The fact that the PulG-like pseudopilins lack this structural feature and do not show the substantial sequence variation typical of authentic type IV pili suggests that they are not normally exposed to selective pressures (bacteriophages, antibodies) in the environment. This would be in agreement with the proposal that pili formed by pseudopilins are artefacts resulting from the uncontrolled elongation of a normally shorter, periplasmic pseudopilus formed *in vivo* (Sauvonnet *et al.*, 2000a; Vignon *et al.*, 2003), which is induced by artificially induced, high level expression of the pseudopilin. Thus, although their structure is of biological interest, any properties associated with these pili (such as improved biofilm formation) (Durand *et al.*, 2003; Vignon *et al.*, 2003) are probably not physiologically relevant.

Because the overall structure of the PulG monomer is similar to that of type IV pilins, it is instructive to compare the different molecular architectures proposed for the pili that they form. The data presented here clearly show that PulG packs into a flexible, one-start, left-handed helical structure with a monomeric building block [the observed dimer in the crystal packing of the truncated monomer (Fig. 4) is considered to be a crystallization artefact] as proposed for several type IVa pilins. The pitch of these filaments was $(4.38 \pm 0.12\ \text{nm})^{-1}$. Compatible with their inherent flexibility (compare the rigid structure of type 1 pili) (Hahn *et al.*, 2002), the helical symmetry of the PulG pili varied depending on the filament stretch tested. The rule best describing the average situation is $l = 4n + 17m$ ($\psi = 84.7°$). Accordingly, we propose that the left-handed pilus filament has a repeat of four helical turns composed of 17 monomeric PulG subunits.

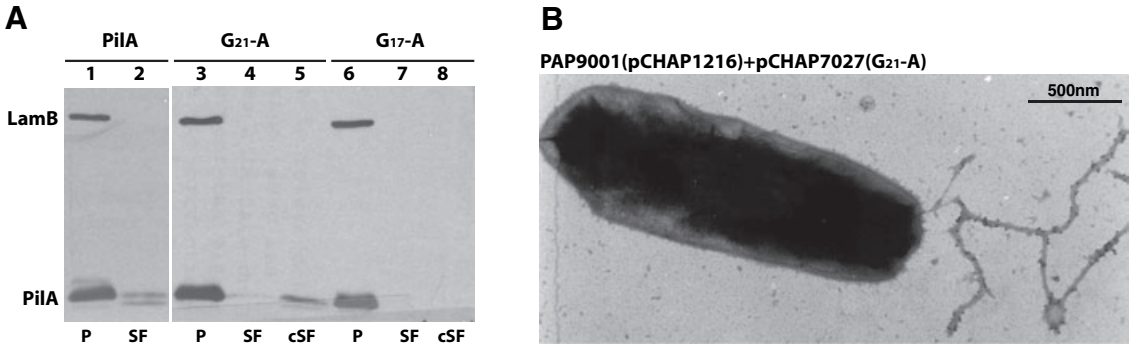

Fig. 9. A. Western blot of PAP9001(pCHAP1216) carrying pCHAP1379(PilA^{PAK}), pCHAP7027(G_{21}-A^{PAK}) or pCHAP7026(G_{17}-A^{PAK}) probed with antisera against PilA^{PAK} and LamB.
B. Immuno-EM of PAP9001(pCHAP1216) + pCHAP7027(G_{21}-A^{PAK}), probed with anti-PilA^{PAK} antibodies followed by secondary antibodies coupled to 5 nm gold beads.

Pseudomonas aeruginosa pseudopilin XcpT, a close homologue of PulG, forms pili whose structure has also been analysed by electron microscopy (Durand *et al*., 2003). Like PulG pili, XcpT pili have helically arranged side projections that were proposed to correspond to the extreme C-terminal region of XcpT and to be implicated in knob and crevice interactions (Durand *et al*., 2003) that cause the bundling characteristic of all PulG/XcpT-like pili examined to date (Vignon *et al*., 2003). This assignment is in agreement with the proposed atomic model of PulG pili and experimental data showing the extreme C-terminus of PulG to be on the outside of the PulG pilus (Vignon *et al*., 2003). Furthermore, the fact that the C-terminal His tag of PulG(His)^6 is not resolved in the crystal structure suggests that it is unstructured, which might explain the failure of these pili to form bundles (Vignon *et al*., 2003), although extension of the PulG C-terminus by other short peptides does not abolish bundling (Vignon *et al*., 2003).

Models of type IV pili based on X-ray crystallography, NMR, fibre diffraction and electron microscopic data also consistently show helical arrangements. Nevertheless, the models differ. The now extensive data on the heterologous assembly of type IV pilins should be taken into account when considering the respective merits of these different models. For example, PilE from *N. gonorrhoeae* can be assembled by *P. aeruginosa* that normally produces pili containing the endogenous type IV pilin PilA^{PAK} (Hoyne *et al*., 1993). This would be consistent with the proposal that both of these proteins pack into right-handed helical pili (Parge *et al*., 1995; Craig *et al*., 2004), although left-handed models for PilA pili have also been proposed (Hazes *et al*., 2000; Keizer *et al*., 2001; Craig *et al*., 2003). *P. aeruginosa* can assemble several other

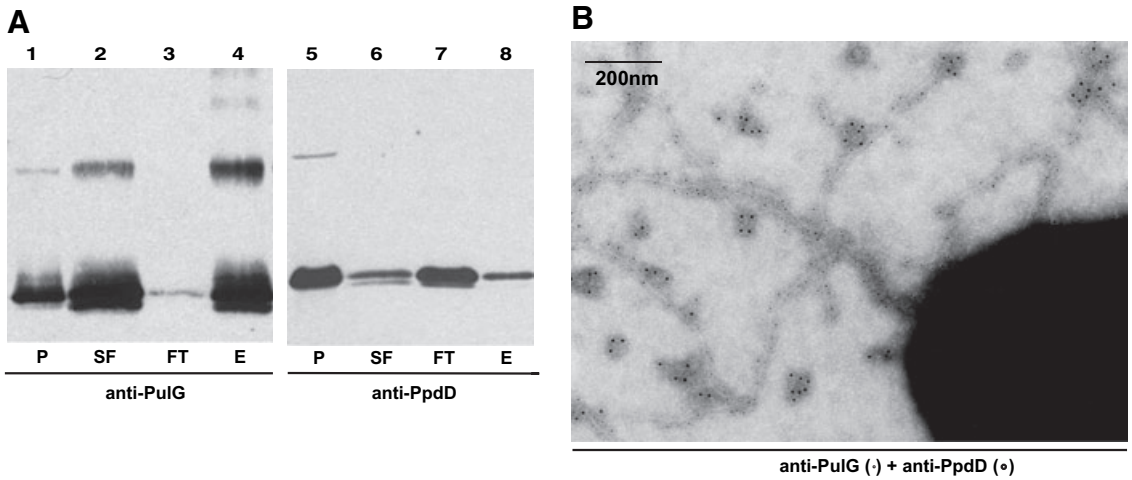

Fig. 10. A. Immunoblot of affinity-purified PulG(His)^6 pili from strain PAP9001(pCHAP7003) constitutively coexpressing *pulG::His*^{6} and *ppdD* and carrying (pCHAP1216(*ΔpulG*)). Lanes 1, 5: (P) pellet; 2, 6: (SF) sheared fraction; 3, 7: (FT) flow-through from affinity column; 4, 8: (E) eluted fraction from affinity column. Membranes were probed with antibodies directed against PulG (lanes 1–4) or PpdD (lanes 5–8).
B. Immuno-EM analysis of pili labelled with anti-PulG antibodies and secondary antibodies coupled to 5 nm gold beads, and then with anti-PpdD and secondary antibodies tagged with 10 nm gold beads.

type IV pilins (Elleman *et al*., 1986; Elleman and Peterson, 1987; Beard *et al*., 1990), including PpdD from *E. coli* K-12 (Sauvonnet *et al*., 2000b). Interestingly, PpdD can also be assembled by the Pul secreton (Sauvonnet *et al*., 2000a), and yet our data indicate that PulG, which is assembled by the same secreton, forms a left-handed helical pilus (Fig. 6). Furthermore, $PilA^{PAK}$ and PilE can both be assembled by the Pul secreton, although with low efficiency, when parts of their N-terminal hydrophobic α-helices are replaced by the corresponding segment of pseudopilin PulG. These substitutions are most unlikely to affect the pitch of the pili formed by $PilA^{PAK}$ and PilE. Thus, we must conclude either that the same machinery is able to assemble both left- and right-handed pili, depending on the pseudopilin/pilin it produces or that one of the proposed models (left- or right-handed pitch) is incorrect.

The fact that the native forms of neither PilE nor $PilA^{PAK}$ were assembled by the Pul secreton could result from incompatibility between the assembly machinery and the globular head domain or the N-terminal helix of these pilins. The latter is positioned in the centre of the pilus in all currently available molecular models for type IV pili. This region of the pilin monomer is proposed to be involved in substantial subunit interactions that facilitate pilus formation. When not assembled, the same region of the protein anchors the pilin subunits in the membrane and it is also reasonable to assume that it is required for pilin export (possibly by the Sec pathway). Replacement of the first 17 or 21 amino acids of PilE or $PilA^{PAK}$, respectively, by the corresponding region of PulG permitted these pili to be assembled by the Pul secreton (Table 5). Furthermore, a chimera containing the first 17 amino acids of PilE followed by PulG [chimera E_{17}-G$(His)^6$ in Table 5] both was assembled into pili when overproduced and promoted pullulanase secretion, implying that the N-terminal region of PilE can replace the corresponding region of PulG without affecting PulG function. These data, together with the surprising failure of the Pul secreton to assemble chimeras formed by replacing the N-terminal hydrophobic region of PpdD by the corresponding region of PulG, suggest that this region of the pilin/pseudopilin must be structurally compatible with the rest of the polypeptide to which it is fused for export or assembly to occur. Similar constraints have already been found to apply to heterologous combinations of signal peptide and exported proteins in bacteria (Pugsley, 1993a).

Even relatively minor mutation-induced sequence changes in the hydrophobic helix PulG or PilA disrupt their ability to promote secretion (PulG) or to form pili ($PilA^{PAK}$ and PulG) (Pugsley, 1993b; Strom *et al*., 1993; Vignon *et al*., 2003), but few attempts have been made to identify the step at which the mutation-induced step is blocked (export, retention in the membrane or assembly). The exception is the mutation affecting the totally conserved glutamate at position +5 (E+5) in the hydrophobic α-helix, which is missing from $PulG_{25\text{-}134}(His)^6$. E+5 is required for PilA assembly (Pasloske and Paranchych, 1988; Pasloske *et al*., 1989; Strom and Lory, 1991) and for PulG function in secretion (Pugsley, 1993b), but not for cleavage by prepilin peptidase (Strom and Lory, 1991; Pugsley, 1993b) or for PulG assembly into pili (Vignon *et al*., 2003). In the structure of $PilA^{PAK}$ with the complete N-terminus (Craig *et al*., 2003), E+5 is positioned such that its side-chain could form a salt bridge with the N-terminal phenylalanine. In addition, E+5 in PilA is required for *N*-methylation of the N-terminal phenylalanine (Pasloske and Paranchych, 1988; Strom and Lory, 1991) but this is not the case in PulG (Pugsley, 1993b). The experimentally determined MPL, 15.5 ± 0.8 kDa nm^{-1}, corresponds very closely to one PulG$(His)^6$ monomer per nm. How does this fit with the type IV pilus model (Craig *et al*., 2003), which proposes the existence of a salt bridge between the N-terminal amino group of one pilus monomer and the ε-oxygens of the E+5 residue of the subsequent monomer? In an α-helix, the rise per five residues is only 0.75 nm but this distance could be increased to 1 nm with a suitable side-chain conformation of the E+5. Therefore, a salt bridge could also stabilize the PulG pilus or facilitate the dynamic assembly and disassembly of the pseudopilus during secretion (Vignon *et al*., 2003). More extensive analyses of this and other sequence constraints on the N-terminal regions of PulG and type IV pilins could be very instructive. Other aspects of the proposed atomic model of the PulG pilus must also be verified, for example, by analysing both the surface exposure of residues that are predicted to be on the outside of the pilus and the importance of other amino acids predicted to be involved in subunit interactions, as was performed for the TcpA pilus (Sun *et al*., 1991; 1997; Kirn *et al*., 2000; Craig *et al*., 2003).

Although pseudopilins/type IV pilins have similar overall structural organization, they still differ considerably. The structure of PpdD is not known but it is unlikely to be any more similar to PulG than is PilE or PilA. Therefore, it is not surprising that it cannot be assembled into the same pilus as PulG. What is surprising, however, is that PpdD does not assemble into regular pilus-like structures when coexpressed with PulG. Instead, the protein seems to form ill-defined clusters that associate with bundled PulG pili (Sauvonnet *et al*., 2000a) or with the single pili formed by PulG$(His)^6$ (this study). More detailed analysis of this phenomenon indicated that PulG is more efficiently assembled by the Pul secreton than is PpdD (not shown), suggesting that the failure of PpdD to form pili in cells producing PulG results from its inability to compete efficiently with PulG for access to the export/assembly machinery.

The studies reported here represent a structural basis for exploring the role of PulG in secretion. The pilus formed by pseudopilins is proposed to represent an aberrant variant of a pseudopilus that is usually restricted to the periplasm and might function as a dynamic motor or piston that pushes secreted proteins through the secretin channel in the outer membrane. The validation of this hypothesis will require analysis of the way pilus growth and retraction are promoted and regulated, of how the minor pseudopilin PulI promotes pilus PulG assembly (Sauvonnet *et al*., 2000a), of how PulK performs its proposed role in the control of (pseudo)pilus length (Vignon *et al*., 2003) and of the specific role of PulJ in secretion. Structure analysis of these proteins and studies of their ability to interact with the PulG pilus that are currently underway will provide valuable insight into this fascinating secretion machine.

Experimental procedures

Strains and growth conditions

Escherichia coli strains are listed in Table 1. Bacteria were grown at 30°C in Luria–Bertani (LB) broth (Miller, 1992) or on LB agar plates supplemented, where appropriate, with maltose (0.4%), chloramphenicol (25 μg ml^{-1}) or ampicillin (50 or 100 μg ml^{-1}).

DNA manipulations and plasmids

The sequence encoding for the N-terminal truncated PulG gene from position +25 relative to the prepeptide cleavage site was amplified by standard polymerase chain reaction (PCR) reactions using pCHAP1362 as template. Primers used for amplification were 5′PulG(*Nco*I) 5′-CCC AAC CCC ATG GGC AAC AAG GAA-3′ and 3′PulG(*Xba*I) 5′-CAT CTC TAG AAA CGT AAA GCC GCG-3′. The restriction sites used to fuse the fragment to the signal peptide of *E. chrysanthemi* pectate lyase PelB (PelB^{SP}) in pCHAP4260 (Ap^r) are underlined and resulted in pCHAP7010. The entire fragment encoding PelB^{SP}-PulG$_{25\text{-}134}$(His)^6 was subcloned into pSU18(Cm^r) using *Eco*RI and *Hin*dIII, giving pCHAP7012 that was used to test complementation and transdominant effects in a pullulanase secretion assay (Michaelis *et al*., 1985). For higher level production, the same fragment was subcloned into the overexpression vector pT7-5 (Tabor and Richardson, 1985), giving pCHAP7013.

Plasmid pCHAP7009 (Δ*pulG*, Δ*pulA*) was constructed in order to purify full-length PulG without co-purifying PulA. pCHAP1216, a Δ*pulG* variant of pCHAP231, was digested using *Eco*RI and *Hin*dIII to release a ~12 kb fragment carrying all pul genes between *pulB* and *pulF*. The fragment was subcloned into pUC19, giving plasmid pCHAP7007. *Bam*HI digestion was used to release two internal *pulA* fragments from pCHAP7007. The remaining vector sequence encoding *pulB-ΔpulA-pulF* was gel purified and religated giving pCHAP7008. Finally, the entire fragment was released from pCHAP7008 by digestion with *Eco*RI and *Hin*dIII and reintegrated into pCHAP1216 cut with *Eco*RI and *Hin*dIII (*pulF-pulO*), resulting in pCHAP7009.

pCHAP1404 and pCHAP1418 (*pilE* and *tcpA* respectively) were constructed by amplifying DNA from plasmids pPilEN400 (M. Koomey) and pRT198 (R. Taylor), respectively, using primers that flanked the pilin gene and that introduced sites (*Eco*RI and *Hin*dIII and *Xba*I and *Hin*dIII respectively) that permitted their oriented insertion into the corresponding sites of pSU18 or pSU19 (Bartolomé *et al*., 1991). In both cases, the 5′ oligonucleotide was designed to permit in frame fusion to the first few codons of the *lacZ* gene in the vector to ensure efficient translation initiation in *E. coli* (Table S2). The resulting proteins were readily detectable with antibodies against PilE and TcpA respectively. pCHAP1379 (*pilA*) was obtained by direct subcloning of a 1 kb *Hin*dIII fragment from pAW103 (J. Mattick) into pSU18 so that the gene was under *lacZ*p control.

Polymerase chain reactions with overlapping primer pairs (Table S3) were used to generate gene fusions encoding for hybrids of which the N-terminal α-helix up to and including positions +17, +21 or +26 (relative to the prepeptide cleavage site) and the hydrophilic region of PulG, PpdD, PilE and PilA^{PAK} (downstream from position +18, +22 and +27) were exchanged. Sequences encoding chimeras were first amplified in two fragments using either oligonucleotides 1 and 2 or oligonucleotides 3 and 4 and the appropriate template DNA (Table S3). Fragments were then amplified using standard PCRs with Herculase (Stratagene) and purified using QIAquick columns (Qiagen). Fragments to be fused were heated for 2 min to 92°C and then held at room temperature to allow hybridization. These samples were used as templates in a nested PCR to amplify the entire fusion fragment using only the outer 5′ (1) and 3′ (4) primers. Subsequently, the PCR product was gel purified and digested with restriction enzymes cleaving cognate sequences introduced by the oligonucleotides, and the fragments were cloned into pSU18. The domain exchanges were confirmed by DNA sequencing.

Periplasmic extraction and purification of PelB^{SP}-PulG$_{25\text{-}134}$(His)^6

To produce PelB^{SP}-PulG$_{25\text{-}134}$(His)^6, *E. coli* BL21(DE3) (F$^-$ *ompT lon hsdS$_B$*, λDE3; carries phage T7 DNA polymerase gene under *lacZ*p control) transformed with pCHAP7013 was grown overnight in LB medium at 30°C. All subsequent preparation and incubation steps were carried out on ice and centrifugation was carried out at 4°C. The cells were resuspended in 10 mM Tris/HCl (pH 7.4) containing 20% sucrose and 20 mM EDTA and incubated for 10 min. Bacteria were centrifuged (20 000 *g* for 5 min), resuspended in 25 mM $MgCl_2$ and held for another 10 min. The cells were then centrifuged (20 000 *g* for 5 min). PelB^{SP}-PulG$_{25\text{-}134}$(His)^6 in the supernatant was affinity purified (Vignon *et al*., 2003) and eluted fractions were pooled and dialysed overnight twice against 10 mM Hepes (pH 7.4) using Spectra/Por membranes with a size cut-off of 3.5 kDa. After dialysis, the protein solution was concentrated to 4 mg ml^{-1} using Centriprep and Centricon devises (YM-10) with a size cut-off of 10 kDa. Selenomethionine-labelled PelB^{SP}-PulG$_{25\text{-}134}$(His)^6 was prepared from the same strain grown in minimal medium con-

taining M63 stock salts (Miller, 1992) with glucose (0.2%) and amino acids (4 mg ml^{-1}) except methionine, which was added in the form of selenomethionine to a final concentration of 4 mg ml^{-1}.

Shearing and immunoblotting

Bacteria were harvested from the plates and resuspended in phosphate-buffered saline to an optical density of 1.0 (SF) or 2.0 (cSF) at 600 nm. The suspension was centrifuged twice at 13 000 *g* in a microcentrifuge for 5 min (each time) to separate bacteria (the pellet fraction) from the pilus-enriched supernatant (sheared fraction). Fractions were precipitated with 10% trichloroacetic acid and loaded onto sodium dodecyl sulphate (SDS)-12% polyacrylamide gels for immunoblotting. Proteins were separated by SDS-polyacrylamide gel electrophoresis (PAGE), electroblotted onto nitrocellulose membranes, and incubated first with specific anti-serum [polyclonal anti-PulG at 1/6000, anti-PpdD at 1/1000, anti-PilE at 1/4000 (M. Koomey), anti-$PilA^{PAK}$ at 1/1000 (S. Lory) and anti-LamB at 1/5000] and then with horseradish peroxidase-coupled anti-rabbit or anti-mouse immunoglobulin G (1/10 000; Amersham). The membranes were developed by enhanced chemiluminescence (Amersham). Procedures for transmission electron microscopy were essentially as used previously (Sauvonnet *et al*., 2000a), with specific antibodies diluted to 1:100 and with 10 nm or 5 nm gold beads coupled to the secondary antibodies. Specimens were analysed as described elsewhere (Vignon *et al*., 2003).

Gel filtration

The assembly state of full-length PulG and of soluble truncated PulG were determined by FPLC size-exclusion chromatography with a Superose12 (24 ml) column (Pharmacia) equilibrated with 50 mM phosphate buffer (pH 7.0) containing 150 mM NaCl and 0.7% C_8E_4. Molecular sizes were estimated from standards purchased from Sigma (bovine serum albumen, 66 kDa, and carbonic anhydrase, 29 kDa).

Freeze drying and metal shadowing

Five microlitre aliquots of the sample were adsorbed to glow-discharged carbon-coated collodion films on 400 mesh/inch copper grids, washed on four drops of water and, after removal of excess liquid, frozen by plunging into liquid nitrogen. Freeze drying was performed in a BAF 300 freeze-fracture device (Balzers AG, Liechtenstein) for 1 h at a sample temperature of –80°C followed by 1 h at –35°C, and a pressure of $\leq 5 \times 10^{-7}$ Torr. Finally, the grids were unidirectionally metal shadowed with tungsten/tantalum (W/Ta) at an elevation angle of 45° to yield an average metal film thickness of ≈ 1 nm, and reinforced with carbon to avoid rehydratation and oxidation of the metal film.

The grids were examined and photographed in a Hitachi H-7000 transmission electron microscope operating at 100 kV. Electron micrographs were recorded at ×30 000 nominal magnification on Kodak SO163 sheet film.

STEM

A Vacuum Generators (East Grinstead) HB-5 STEM, interfaced to a modular computer system (Tietz Video and Image Processing Systems), was used. All samples were prepared on 200-mesh-per-inch gold-plated copper grids as described previously (Müller *et al*., 1992). Isolated tobacco mosaic virus particles (kindly supplied by R. Diaz-Avalos) adsorbed to a separate grid and air-dried, served as mass standard for the measurements.

For structural analysis, digital 512×512 pixel dark-field images were recorded from the isolated negatively stained pili at an acceleration voltage of 100 kV and a nominal magnification of 500 000× using doses of $(7.6 \pm 1.2) \times 10^3$ electrons nm^{-2}. The pixel size is dependent on the focus conditions for the STEM (Müller *et al*., 1992) and was 0.330 ± 0.004 nm for the images analysed.

For mass determination 512×512 pixel dark-field images were recorded from unstained samples of the isolated pili at an acceleration voltage of 80 kV and a nominal magnification of 200 000× using doses of 414 ± 36 electrons nm^{-2}. In addition, repeated low-dose scans were recorded from some grid regions to assess beam-induced mass loss. The images were evaluated with the program package IMPSYS as described previously (Müller *et al*., 1992). Accordingly, pilus segments were defined by square boxes, tracked and their length and mass profile calculated. The total scattering within an integration box matched to their width was then determined, the background scattering of the carbon support film subtracted and the average MPL calculated. Furthermore, the FWHM was determined from the mass profile. The beam-induced mass loss was calculated as described previously (Müller *et al*., 1992). The experimental MPL results were then multiplied by the correction factor calculated for the recording dose used, scaled according to the MPL measured for TMV particles. Finally, the MPL and FWHM values were binned into histograms and fitted with Gauss curves. The overall experimental uncertainty of the MPL average was estimated from the corresponding SE ($SE = SD/\sqrt{n}$) and the 5% uncertainty in the calibration of the instrument by calculating the square root of the sum of the squares.

Digital image processing

Using the SEMPER program package (Saxton *et al*., 1979), suitable negatively stained pilus stretches were computationally unbent using a cubic spline interpolation scheme as described previously (Hahn *et al*., 2000). To estimate the outer pilus diameter, selected unbent pili were averaged along their axis and the resulting intensity profile was plotted. The distance between the two outer minima of this profile was taken as the outer diameter. Power spectra were calculated for the unbent pilus segments and the altitude of the most prominent layer line was determined. Layer lines were extracted from the 2D Fourier transforms of the unbent rods to inspect the amplitudes and phases.

Further processing was performed using the Modular Micrograph Data Processing Program (MDPP; Smith and Gottesman, 1996). First, the pitch of well-preserved pili was also determined in real space using the linear Markham superposition procedure described previously (Hahn *et al*.,

2000). Averaging runs were made over two, three and four repeat lengths respectively. In each case, the repeat length was incremented in steps of one pixel until the maximum possible length had been attained (limited by the pilus length). The degree of enhancement on superposition and averaging was quantified by comparing the resulting rms deviation with that of the segment used, whereby maximum values of the quotient correspond to minimal 'blurring' of the average image, i.e. minimum power loss and, thus, to the optimal enhancement of the true repeat. The rms quotient was then plotted for each repeat length and the local maxima assessed graphically.

All helical selection rules falling within the range compatible with helical repeats less than or equal to 10 times the pitch and including screw angles within the range of 72°–90° were compared in batches. For this, the straightened pilus segments were trimmed to an integer multiple of the helical repeat and interpolated onto the sampling grid calculated to give four pixels per axial rise. The width of the filament array was trimmed to minimize the background effect of the negative stain, and the six marginal pixels on either side of the array parallel to the pilus axis were floated to the mean density value. The 2D Fourier transform was calculated and $D(Z,k)$ filtered as described (Smith and Aebi, 1974). At this stage 16 Bessel coefficients and the number of layer lines indicated by the rule under test were used. The rules within a batch were tested on exactly the same stretch of pilus, allowing the results to be compared, e.g. the rule $l = 1n + 5m$ was in the same batch as the rule $10n + 43m$ and the total filament length tested was 260 pixels. Thus for the first rule there were 20 helical repeats and for the second only two.

A stack of 200 sections of 52×52 pixels and spaced by 0.26 nm was calculated from the $D(Z,k)$-filtered layer lines resulting from nine helical repeats containing 153 subunits of one well-preserved pilus rod by back-transformation. This reconstruction comprised 50 axial repeats. It was isocontoured to include 100% of the nominal mass taking a density of 810 Da nm^{-3} into account.

Crystallization and data collection

Small hexagonal bipyramidal crystals of N-terminal truncated $PulG_{25\text{-}134}(His)^6$ ($50\ \mu m \times 50\ \mu m \times 70\ \mu m$) were obtained by the hanging drop vapour diffusion method. Two microlitres of 20 mg ml^{-1} purified $PulG_{25\text{-}134}(His)^6$ in 10 mM Hepes pH 7.2, 0.02% (w/v) sodium azide were mixed with 2 µl of reservoir solution containing 1.7 M ammonium sulphate and 5% (v/v) isopropanol as precipitants. These crystals could be enlarged by macro seeding to a final size of $200\ \mu m \times 200\ \mu m \times 300\ \mu m$ by transferring them into a new drop composed of 2 µl of protein solution (30 mg ml^{-1}) and 2 µl of reservoir [1.6 mM ammonium sulphate, 5% (v/v) isopropanol]. The space group was found to be $P6_522$ with cell dimensions of 85.4 Å for the *a*/*b*-axis and 145.7 Å for the *c*-axis.

Crystals of selenomethionine-containing $PulG_{25\text{-}134}(His)^6$ were grown and analysed to resolve the crystallographic phase problem. Well-diffracting derivative crystals of the same space group grew in hanging drops containing 2 µl of selenomethionine $PulG_{25\text{-}134}(His)^6$ 15 mg ml^{-1} in 10 mM Hepes pH 7.2, 0.02% (w/v sodium azide) and 2 µl of the reservoir [1.9 M ammonium sulphate, 6.5% (v/v) isopropanol].

Diffraction data were collected under cryogenic conditions. The crystals were flash frozen in liquid nitrogen in buffer corresponding to the equilibrated crystallization drops plus 25% (v/v) glycerol as a cryoprotectant. Two data sets from one native $PulG_{25\text{-}134}(His)^6$ crystal were collected: one on a rotating anode X-ray source equipped with a Mar345 detector and one high resolution data set at the Swiss-Light-Source (SLS, beamline X06SA) provided with a MarCCD detector. Both data sets were processed using XDS2002 (Kabsch, 1993) and subsequently merged in XSCALE2002.

Data from one derivative crystal were collected at the SLS at two different wavelengths, corresponding to the remote high value and the inflection point of the anomalous signal from the covalently bound selenium atoms. These data sets were also reduced using XDS2002. More details of the data collection statistics are shown in Table 3.

Crystal structure determination and refinement

The crystallographic phase problem was solved by multiple anomalous dispersion (MAD). Two strong and a further four less occupied heavy atom positions were found in the derivative crystal using the program SHELXD (Schneider and Sheldrick, 2002). All of them were taken as selenium atoms for experimental phase determination. The calculated phases were combined with the intensities from the merged native data set and extended to 1.8 Å in SHELXE. This resulted in an interpretable electron density map (final weighted contrast 0.71, connectivity 0.95 as given by SHELXE).

Model building and refinement was done with programs of the CCP4-suite (Collaborative Computational Project, 1994) and the graphical model building program 'O' (Jones *et al.*, 1991) for visible inspection and manual improvement of the model. A starting model consisting of 199 peptides distributed over 6 separated chains was obtained by automatic model building with the program ARPWARP (Perrakis *et al.*, 1999) using the extended experimental phases and all native data. It clearly corresponds to a dimer in the asymmetric unit. Side-chain atoms as well as other missing parts of the structure were added manually, followed by alternating refinement cycles including non-crystallographic symmetry restraints and anisotropic B-factor refinement in REFMAC5 (Murshudov *et al.*, 1997; 1999). Solvent atoms were added automatically by the program ARPWARP (Lamzin and Wilson, 1993). Model statistics are summarized in Table 4.

Modelling of the PulG pilus

The monomer derived from the crystal structure was prepared for helical modelling as follows: (i) the C-terminal section (amino acids N128-G132) including β-strand S4 which forms the interdomain contact in the crystallographic dimer was relocated into its monomer by removing the second monomer of the asymmetric unit, (ii) the flexible hinge region composed of I126 and G127 was modelled with the SWISS-MODEL server (http://www.expasy.org/swissmod/SWISS-MODEL.html) and (iii) the N-terminal α-helix was

elongated. For this, the backbone of the 24 missing residues were taken from the N-terminal helix of the $PulG_{25–134}(His)^6$ structure and manually moved to the corresponding position in the graphical model building software 'O'. Side-chain positions were taken as the standard conformations proposed by the program 'O'.

Modelling was performed using the visualization tool DINO (http://www.dino3d.org), which allows the display of helical symmetry mates as well as their synchronous real-time update upon rotation and translation of the reference monomer. Constraints applied during the modelling procedure were: (i) helical symmetry according to the performed analysis: rotation angle of ±84.71 degree per subunit and an axial rise of 1.04 nm, (ii) the long α-helix was located within the core of the pilus helix, both axes quasi-parallel, (iii) the C-terminus was exposed to the outside medium and (iv) compact packing was ensured visually, avoiding steric clashes and cavities within the pilus core.

Acknowledgements

We would like to thank Marie-Christine Prévost for her guidance and permission to use the facilities at the Electron Microscope Station at the Institut Pasteur, Michael Koomey, Steve Lory, John Mattick and Ron Taylor for plasmids and/or antibodies and Vesna Olivieri for the STEM microscopy. We also thank Erik Hahn, Michel Steinmetz and Ueli Aebi for their help in the use of the helical processing programs. The European Commission (Contract No. HPRN-2000-00075), the Maurice E. Müller Foundation of Switzerland and the Swiss National Foundation contributed financially to this work.

Supplementary material

The following material is available from
http://www.blackwellpublishing.com/products/journals/suppmat/mmi/mmi4307/mmi4307sm.htm

Appendix A1. The supplementary material includes structural and functional data on the PulG pilus and control data on the failure of the Pul secreton to assemble the TcpA pilus.

Fig. S1. The metal binding site in the dimeric crystal form of $PulG_{25-134}(His)^6$.

Fig. S2. Processing of preTcpA in *E. coli* strain carrying the prepilin peptidase structural gene *pulO*.

Fig. S3. Analysis of pellet and sheared fractions of *E. coli* stains PAP7000BG, PAP7501(pCHAP1216) and PAP9001(pCHAP1216) carrying pCHAP3100 (*ppdD*), pCHAP7023 and pCHAP7019 (encoding G_{17}-D and G_{21}-D respectively) by immunoblotting.

Fig. S4. Multiple sequence alignment of the first 23 N-terminal amino acids of PulG, PilE, $PilA^{PAK}$ and PpdD.

Fig. S5. Western blot analysis of bacterial pellet, sheared fractions and concentrated sheared fractions from *E. coli* K-12 strain PAP7500BG(Δ*pulG*) harbouring pCHAP3100 (encoding PpdD) (lanes 1–3) and pCHAP7028 (encoding $G_{21(modified)}$-D) (lanes 4–6) respectively.

Fig. S6. A structural alignment of the C-terminal globular domain of the pseudopilin PulG with known type IV pilin structures.

Table S1. Similarity of atomic structures of type IV pilins and PulG. The structures were superimposed with the program LSQMAN as described in Fig. S2.

Table S2. Oligonucleotide primers used to amplify *pilE* and *tcpA* genes.

Table S3. Oligonucleotide primers used to construct pilin/pseudopilin chimeras in which the N-terminal domains were interchanged.

References

Bartolomé, B., Jubete, Y., Martinez, E., and de la Cruz, F. (1991) Construction and properties of a family of pACYC184-derived cloning vectors compatible with pBR322 and its derivatives. *Gene* **102:** 75–78.

Beard, M.K., Mattick, J.S., Moor, M.R., Marrs, C.F., and Egerton, J.R. (1990) Morphogenic expression of *Moraxella bovis* fimbriae (pili) in *Pseudomonas aeruginosa*. *J Bacteriol* **172:** 2601–2607.

Bitter, W., Koster, M., Latijnhouwers, M., de Cock, H., and Tommassen, J. (1998) Formation of oligomeric rings by XcpQ and PilQ, which are involved in protein transport across the outer membrane of *Pseudomonas aeruginosa*. *Mol Microbiol* **27:** 209–219.

Brok, R., Van Gelder, P., Winterhalter, M., Ziese, U., Koster, A.J., de Cock, H., *et al.* (1999) The C-terminal domain of the *Pseudomonas* secretin XcpQ forms oligomeric rings with pore activity. *J Mol Biol* **294:** 1169–1179.

Collaborative Computational Project (1994) The CCP4 suite: programs for protein crystallography. *Acta Cryst* **D50:** 760–763.

Collins, R.F., Davidsen, L., Derrick, J.P., Ford, R.C., and Tonjum, T. (2001) Analysis of the PilQ secretin from *Neisseria meningitidis* by transmission electron microscopy reveals a dodecameric quaternary structure. *J Bacteriol* **183:** 3825–3832.

Collins, R.F., Ford, R.C., Kitmitto, A., Olsen, R.O., Tonjum, T., and Derrick, J.P. (2003) Three-dimensional structure of the *Neisseria meningitidis* secretin PilQ determined from negative-stain transmission electron microscopy. *J Bacteriol* **185:** 2611–2617.

Craig, L., Taylor, R., Pique, M.E., Adair, B.D., Arvai, A.S., Singh, M., *et al.* (2003) Type IV pilin structure and assembly. X-ray and EM analyses of *Vibrio cholerae* toxin-coregulated pilus and *Pseudomonas aeruginosa* PAK pilin. *Mol Cell* **11:** 1139–1150.

Craig, L., Pique, M.E., and Tainer, J.A. (2004) Type IV pilus structure and bacterial pathogenicity. *Nature Rev Microbiol* **2:** 363–378.

DeRosier, D.J., and Klug, A. (1968) Reconstitution of three-dimensional structures from electron micrographs. *Nature* **217:** 130–134.

Diederichs, K., and Karplus, P.A. (1997) Improved R-factors for diffraction data analysis in macromolecular crystallography. *Nature Struct Biol* **4:** 269–275.

Dupuy, B., Taha, M.-K., Possot, O., Marchal, C., and Pugsley, A.P. (1992) PulO, a component of the pullulanase secretion pathway of *Klebsiella oxytoca*, correctly and efficiently processes gonococcal type IV prepilin in *Escherichia coli*. *Mol Microbiol* **6:** 1887–1894.

Durand, E., Bernadac, A., Ball, G., Lazdunski, A., Sturgis,

J.N., and Filloux, A. (2003) Type II protein secretion in *Pseudomlonas aeruginosa*: the pseudopilus is a multifibrillar and adhesive structure. *J Bacteriol* **185:** 2749–2758.

Elleman, T.C., and Peterson, J.E. (1987) Expression of multiple types of N-methyl Phe pili in *Pseudomonas aeruginosa*. *Mol Microbiol* **1:** 377–380.

Elleman, T.C., Hoyne, P.A., Stewart, D.J., McKern, N.M., and Peterson, J.E. (1986) Expression of pili from *Bacteroides nodosus* in *Pseudomonas aeruginosa*. *J Bacteriol* **168:** 574–580.

d'Enfert, C., Ryter, A., and Pugsley, A.P. (1987) Cloning and expression in *Escherichia coli* of the *Klebsiella pneumoniae* genes for production, surface localization and secretion of the lipoprotein pullulanase. *EMBO J* **6:** 3531–3538.

Hagblom, P., Segal, E., Billyard, E., and So, M. (1985) Intragenic recombination leads to pilus antigenic variation in *Neisseria gonorrhoeae*. *Nature* **315:** 156–158.

Hahn, E., Wild, P., Schraner, E.M., Bertschinger, H.U., Häner, M., Müller, S.A., and Aebi, U. (2000) Structural analysis of F18 fimbriae expressed by porcine toxigenic *Escherichia coli*. *J Struct Biol* **132:** 241–250.

Hahn, E., Wild, P., Hermanns, U., Sebbel, P., Glockshuber, R., Häner, M., *et al.* (2002) Exploring the 3D molecular architecture of *Escherichia coli* type 1 pili. *J Mol Biol* **323:** 845–857.

Hazes, B., Sastry, P., Hayakawa, K., Read, R., and Irvin, R. (2000) Crystal structure of *Pseudomonas aeruginosa* PAK pilin suggests a main-chain-dominated mode of receptor binding. *J Mol Biol* **299:** 1005–1017.

Hobbs, M., and Mattick, J.S. (1993) Common components in the assembly of type 4 fimbriae, DNA transfer systems, filamentous phage and protein-secretion apparatus: a general system for the formation of surface-associated protein complexes. *Mol Microbiol* **10:** 233–243.

Hoyne, P.A., Haas, R., Meyer, T.F., Davies, J.K., and Elleman, T.C. (1993) Production of *Neisseria gonorrhoeae* pili (fimbriae) in *Pseudomonas aeruginosa*. *J Bacteriol* **174:** 7321–7327.

Hu, N.-T., Leu, W.-M., Lee, M.-S., Chen, A., Chen, S.-C., Song, Y.-L., and Chen, L.-Y. (2002) XpsG, the major pseudopilin in *Xanthomonas camplestric* pv. campestris forms a pilus-like structure between cytoplasmic and outer membranes. *Biochem J* **365:** 205–211.

Jones, T.A., Zou, J.Y., and Kjeldgard, M. (1991) Improved methods for building protein models in electron density maps and the location of errors in these models. *Acta Cryst* **A47:** 110–119.

Kabsch, W. (1993) Automatic processing of rotation diffraction data from crystals of initially unknown symmetry and cell constants. *J Appl Cryst* **26:** 795–800.

Kabsch, W., and Sander, C. (1983) Dictionary of protein secondary structure: pattern recognition of hydrogen-bonded and geometrical features. *Biopolymers* **22:** 2577–2637.

Keizer, D., Slupsky, C., Kalisiak, M., Campbel, A., Crump, M., Sastry, P., *et al.* (2001) Structure of a pilin monomer from *Pseudomonas aeruginosa*: implications for the assembly of pili. *J Biol Chem* **276:** 24186–24193.

Kirn, T.J., Lafferty, M.J., Sandoe, C.M.P., and Taylor, R.K. (2000) Delineation of pilin domains required for bacterial association into microcolonies and intestinal colonization by *Vibrio cholerae*. *Mol Microbiol* **35:** 896–910.

Lamzin, V.S., and Wilson, K.S. (1993) Automated refinement of protein models. *Acta Cryst* **D49:** 129–149.

Laskowski, R.A., MacArthur, M.W., Moss, D.S., and Thornton, J.M. (1993) PROCHECK: a program to check the stereochemical quality of protein structures. *J App Chryst* **26:** 383–391.

Michaelis, S., Chapon, C., d'Enfert, C., Pugsley, A.P., and Schwartz, M. (1985) Characterization and expression of the structural gene for pullulanase, a maltose-inducible secreted protein of *Klebsiella pneumoniae*. *J Bacteriol* **164:** 633–638.

Miller, J.H. (1992) A short course in bacterial genetics. *A Laboratory Manual and Handbook for Escherichia coli and Related Bacteria.* Cold Spring Harbor: Cold Spring Harbor Laboratory Press.

Müller, S.A., Goldie, K.N., Bürki, R., Häring, R., and Engel, A. (1992) Factors influencing the precision of quantitative scanning transmission electron microscopy. *Ultramicroscopy* **46:** 317–334.

Murshudov, G.N., Vagin, A.A., and Dodson, E.J. (1997) Refinement of macromolecular structures by the maximum-likelihood method. *Acta Cryst* **D53:** 240–245.

Murshudov, G.N., Lebedev, A., Vagin, A.A., Wilson, K.S., and Dodson, E.J. (1999) Efficient anisotropic refinement of macromolecular structures using FFT. *Acta Cryst* **D55:** 247–255.

Nicholls, A., Sharp, K.A., and Honig, B. (1991) Protein folding and association: insights from the interfacial thermodynamic properties of hydrocarbons. *Proteins* **11:** 281–296.

Nouwen, N., Ranson, N., Saibil, H., Wolpensinger, B., Engel, A., Ghazi, A., and Pugsley, A.P. (1999) Secretin PulD: association with pilot protein PulS, structure and ion-conducting channel formation. *Proc Natl Acad Sci USA* **96:** 8173–8177.

Nouwen, N., Stahlberg, H., Pugsley, A.P., and Engel, A. (2000) Domain structure of secretin PulD revealed by limited proteolysis and electron microscopy. *EMBO J* **19:** 2229–2236.

Nunn, D. (1999) Bacterial type II protein export and pilus biogenesis: more than just homologies? *Trends Cell Biol* **9:** 402–408.

Parge, H.E., Forest, K.T., Hickey, M.J., Christensen, D.A., Getzoff, E.D., and Tainer, J.A. (1995) Structure of the fibre-forming protein pilin at 2.6 Å resolution. *Nature* **378:** 32–38.

Pasloske, B.L., and Paranchych, W. (1988) The expression of mutant pilins in *Pseudomonas aeruginosa*: fifth position glutamate affects pilin methylation. *Mol Microbiol* **2:** 489–495.

Pasloske, B.L., Scraba, D.G., and Paranchych, W. (1989) Assembly of mutant pilins in *Pseudomonas aeruginosa*: formation of pili composed of heterologous subunits. *J Bacteriol* **171:** 2142–2147.

Peabody, C.R., Chung, Y.C., Yen, M.R., Vidal-Ingigliardi, D., Pugsley, A.P., and Saier, M.H., Jr (2003) Type II protein secretion and its relationship to bacterial type IV pili and archaeal flagella. *Microbiology* **149:** 3051–3072.

Perrakis, A., Morris, R., and Lamzin, V.S. (1999) Automated protein model building combined with iterative structure refinement. *Nature Struct Biol* **6:** 458–463.

Possot, O., Vignon, G., Bomchil, N., Ebel, F., and Pugsley, A.P. (2000) Multiple interactions between pullulanase secreton components involved in stabilization and cytoplasmic membrane association of PulE. *J Bacteriol* **182:** 2142–2152.

Pugsley, A.P. (1993a) The complete general secretory pathway in gram-negative bacteria. *Microbiol Rev* **57:** 50–108.

Pugsley, A.P. (1993b) Processing and methylation of PulG, a pilin-like component of the general secretory pathway of *Klebsiella oxytoca*. *Mol Microbiol* **9:** 295–308.

Pugsley, A.P. (1996) Multimers of the precursor of a type IV pilin-like component of the general secretory pathway are unrelated to pili. *Mol Microbiol* **20:** 1235–1245.

Pugsley, A.P., and Possot, O. (1993) The general secretory pathway of *Klebsiella oxytoca*: no evidence for relocalization or assembly of pilin-like PulG protein into a multiprotein complex. *Mol Microbiol* **10:** 665–674.

Pugsley, A.P., Bayan, N., and Sauvonnet, N. (2001) Disulphide bond formation in secreton component PulK provides a possible explanation for the role of DsbA in pullulanase secretion. *J Bacteriol* **183:** 1312–1319.

Sandkvist, M. (2001) Biology of type II secretion. *Mol Microbiol* **40:** 271–283.

Sauvonnet, N., Vignon, G., Pugsley, A.P., and Gounon, P. (2000a) Pilus formation and protein secretion by the same machinery in *Escherichia coli*. *EMBO J* **19:** 2221–2228.

Sauvonnet, N., Gounon, P., and Pugsley, A.P. (2000b) PpdD type IV pilin of *Escherichia coli* K-12 can be assembled into pili in *Pseudomonas aeruginosa*. *J Bacteriol* **182:** 848–854.

Saxton, W.O., Pitt, T.J., and Horner, M. (1979) Digital image processing: the Semper system. *Ultramicroscopy* **4:** 343–354.

Schneider, T.R., and Sheldrick, G.M. (2002) Substructure solution with SHELXD. *Acta Cryst* **D58:** 1772–1779.

Smith, P.R., and Aebi, U. (1974) Computer-generated Fourier transforms of helical particles. *J Phys* **7:** 1627–1633.

Smith, P.R., and Gottesman, S.M. (1996) The micrograph data processing program. *J Struct Biol* **116:** 35–40.

Strom, M.S., and Lory, S. (1991) Amino acid substitutions in pilin of *Pseudomonas aeruginosa*. Effect on leader peptide cleavage, amino-terminal methylation, and pilus assembly. *J Biol Chem* **266:** 1656–1664.

Strom, M.S., Bergman, P., and Lory, S. (1993) Identification of active-site cysteines in the conserved domain of PilD, the bifunctional type IV pilin leader peptidase/*N*-methyltransferase of *Pseudomonas aeruginosa*. *J Biol Chem* **268:** 15788–15794.

Sun, D., Seyer, J.M., Kovari, I., Siumrada, R.A., and Taylor, R.K. (1991) Localization of protective epitopes within pilin subunit of *Vibrio cholerae* toxin-coregulated pilus. *Infect Immun* **59:** 114–118.

Sun, D., Lafferty, M.J., Pek, J.A., and Taylor, R.K. (1997) Domains within the *Vibrio cholerae* toxin coregulated pilin sububnit that mediate bacterial colonization. *Gene* **192:** 79–85.

Tabor, S., and Richardson, C.C. (1985) A bacteriophage T7 RNA polymerase/promoter system for controlled exclusive expression of specific genes. *Proc Natl Acad Sci USA* **82:** 1074–1078.

Vignon, G., Köhler, R., Larquet, E., Giroux, S., Prévost, M.-C., Roux, P., and Pugsley, A.P. (2003) Type IV-like pili formed by the type II secreton: specificity, composition, bundling, polar localization and surface presentation of peptides. *J Bacteriol* **185:** 3416–3428.

Wolfgang, M., van Putten, J.P.M., Hayes, S.F., Dorward, D., and Koomey, M. (2000) Components and dynamics of fiber formation define a ubiquitous biogenesis pathway for bacterial pili. *EMBO J* **19:** 6408–6418.